Proceedings of the CAS-CERN Accelerator School: Intensity Limitations in Particle Beams, Geneva, Switzerland, 2–11 November 2015, edited by W. Herr, CERN Yellow Reports: School Proceedings, Vol. 3/2017, CERN-2017-006-SP (CERN, Geneva, 2017)

Coherent Beam–Beam Effects

X. Buffat
CERN, Geneva, Switzerland

Abstract
The models used to consistently describe the dynamics of two charge particle beams in circular colliders are discussed, along with relevant examples and observations. The need to treat the dynamics of both beams in a consistent manner is introduced with emphasis on conditions in which the resulting effects may become an intensity limitation for the collider.

Keywords
Beam dynamics; orbit effects; dynamic β effect; coherent beam-beam modes; beam coupling impedance; Landau damping.

1 Introduction

In order to describe the dynamics of a high-energy particle beam it is convenient to make a distinction between external forces, e.g. magnets, that affect the motion of the individual particles and so-called coherent forces. The coherent forces depend on the beam properties as a whole; therefore, not only is the single-particle motion affected, but the coherent forces are affected in return. The treatment of such systems require a consistent description of the single-particle dynamics and the coherent forces. The space-charge force is a well-known example of such a coherent force, the aspects of which are discussed in Ref. [1]. The fact that the beam–beam interactions are localized and result from the interaction of two distinct beams reveals several differences with respect to space-charge effects, which we discuss in this paper.

There exists configurations for which the coherent effects of beam–beam interactions remain negligible, i.e. when the beam–beam forces are not strong enough to generate a significant distortion of the other beam's particle distribution. Such configurations are usually referred to as weak–strong, since at least one of the two beams is weak enough not to affect the dynamics of the strong beam. Here we shall consider so-called strong–strong configurations, when the effect of the two beams on each other is strong enough to have an effect on the beam–beam force itself, and therefore require a consistent treatment of the two beams and their electromagnetic interactions. In Section 2 we shall derive an expression for the coherent beam–beam force, and in Section 3 we shall evaluate its effect on the orbit and optics of the two beams in the strong–strong regime. Section 4 is dedicated to the study of oscillatory solutions around the equilibrium and their stability in the presence of beam coupling impedance.

2 Coherent beam–beam kick

The beam–beam kick on a point-like particle, called the incoherent beam–beam kick, can be obtained by integration of Poisson's equation, see Ref. [2]. Using a Gaussian distribution of particles, with r.m.s. transverse beam size $\sigma = \sigma_x = \sigma_y$, one obtains the kick felt by a test particle at a position (x, y) with respect to the other beam's centroid, see Ref. [3]:

$$\Delta x' = -\frac{2r_0 N}{\gamma_r}\frac{x}{r^2}\left(1 - \mathrm{e}^{-r^2/2\sigma^2}\right) , \tag{1}$$

where we have introduced N, the number of charges in the beam, r_0 the classical radius and $r = \sqrt{x^2 + y^2}$. Since the opposing beam is not point-like, the total beam–beam kick, called coherent

https://doi.org/10.23730/CYRSP-2017-003.391

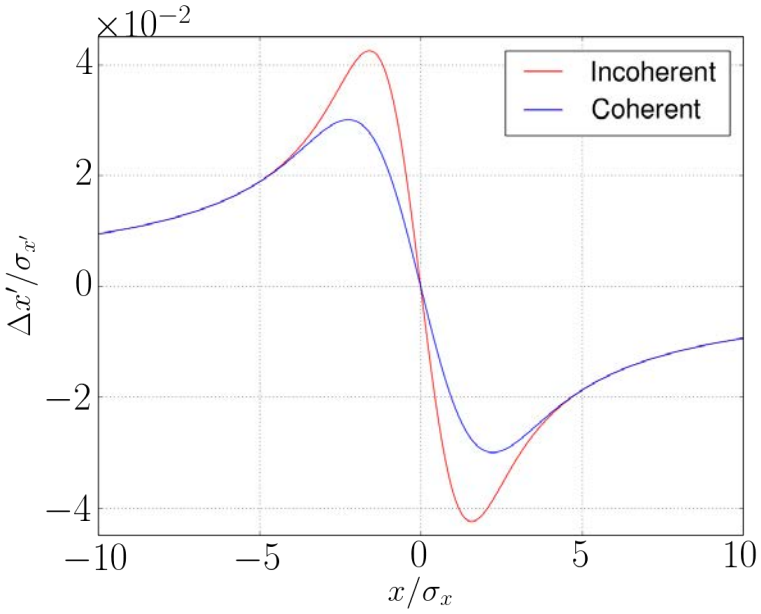

Fig. 1: Comparison between the incoherent and coherent beam–beam kick for round Gaussian beam distributions

kick, is obtained by integration of the single-particle kicks over the beam distribution $\Psi(x, y)$.

$$\Delta x'_{\text{coh}}(x, y) = \int_{-\infty}^{\infty} \mathrm{d}X\mathrm{d}Y \Delta x'(X, Y)\Psi(X - x, Y - y) \, . \tag{2}$$

Assuming a round Gaussian distribution and using Eq. (1), we have, see Ref. [4],

$$\Delta x'_{\text{coh}}(x, y) = -\frac{2r_0 N}{\gamma_r}\frac{x}{r^2}\left(1 - \mathrm{e}^{-r^2/4\sigma^2}\right), \; r = \sqrt{x^2 + y^2} \, . \tag{3}$$

For $x, y \gg \sigma$, we find that the coherent kick is half the single-particle kick, whereas for large separation, i.e for long-range interactions, the difference between coherent and incoherent vanishes (Fig. 1).

3 Self-consistent solutions

In the strong–strong regime, the orbit and optics function of the two beams are dependent on each other through the beam–beam interactions. Therefore a self-consistent calculation of these parameters, including the beam–beam forces, is necessary in order to obtain an accurate description of the two beams. Often, the self-consistent treatment leads to small modifications with respect to a weak–strong treatment, where the beam–beam forces are computed based on the unperturbed optics. In configurations where the beam–beam forces are strong enough, significant dynamic variations of the optics function can occur. We shall illustrate the need for self-consistent solutions through two practical examples: the orbit effect due to multiple long-range beam–beam interactions, and the dynamic β effect.

3.1 Orbit effect

Modern colliders based on synchrotrons usually feature several bunches per beam, potentially leading to several beam–beam interactions per turn. Since head-on collisions other than at the experiment location are unwanted, the beams need to be separated in the rest of the ring. The remaining beam–beam interactions are of long-range type. From Eq. (3), we observe that the coherent kick for beams colliding with

an offset is non-zero, resulting in a modification of the closed orbit, given perturbatively by Ref. [5]:

$$\delta x = \Delta x'_{\text{coh}}(d)\beta \cot(\pi Q) \ , \tag{4}$$

for two beams separated by a distance d in the horizontal plane; for simplicity we assumed $y = 0$. β is the corresponding optics function at the location of the interaction and Q is the unperturbed tune. If the beam–beam interaction is too strong to be treated as a perturbation, i.e. $\Delta_{\text{coh}}(d, 0) \not\approx \Delta_{\text{coh}}(d + \delta x, 0)$, the non-linear equation

$$\delta x = \Delta x'_{\text{coh}}(d + \delta x)\beta \cot(\pi Q) \tag{5}$$

has to be solved. The solution of this equation is, however, not self-consistent, since the effect on the other beam is not taken into account. Considering the two beams self-consistently, one obtains the following system of non-linear equations:

$$\left\{ \begin{array}{rcl} \delta x_1 & = & \Delta x'_{\text{coh}}(d + \delta x_1 + \delta x_2)\beta_1 \cot(\pi Q_1) \\ \delta x_2 & = & \Delta x'_{\text{coh}}(d + \delta x_1 + \delta x_2)\beta_2 \cot(\pi Q_2) \ , \end{array} \right. \tag{6}$$

where the indices refer to the two beams. Such a description is sufficient for configurations where all bunches experience the same beam–beam interactions along the whole ring. This is, however, not the case in machines operated with bunch trains, i.e. where the longitudinal distribution of the bunches along each beam is not uniform. The resulting PACMAN bunches i.e. bunches experiencing different sets of long-range beam–beam interaction, will circulate on different closed orbits (Fig. 2). The algorithm required for the self-consistent evaluation of the orbit of the different bunches is, in essence, identical to the algorithm used to find the closed orbit for a single beam; the dimension of the problem is, however, increased. Starting with a single beam, the closed orbit is defined as the first-order fixed point of a non-linear equation of the following type:

$$\bar{x}_{k+1} = M_0 \cdot \bar{x}_k \ , \tag{7}$$

where M_0 is the one-turn map acting on the phase-space coordinates at a given turn k: $\bar{x_k} = (x_k, x'_k)$. The algorithm can easily be extended to two beams ($i = 1, 2$) with one-turn matrices given by M_1 and M_2 respectively:

$$\bar{x}_{i,k+1} = M_i \cdot \bar{x}_{i,k} \ . \tag{8}$$

In the absence of beam–beam interactions, the one-turn map is identical for all the bunches of each beam:

$$\bar{x}_{i,j,k+1} = M_i \cdot \bar{x}_{i,j,k} \ , \tag{9}$$

with $j = 1, ..., N_b$, the index corresponding to the different bunches of each beam. We can now introduce the effect of beam–beam interactions. The one-turn map of each beam is split into transfer maps between beam–beam interactions, and we write $M_{i,l}$ for the transfer matrix of beam i from beam–beam interaction l to interaction $l+1$, with $l = 1, ..., N_{\text{BB}}$ the index corresponding to the different beam–beam interactions. The effect of the concatenation of the maps must be equal to the original one-turn map:

$$M_i = \prod_{l}^{N_{\text{BB}}} M_{i,l} \ . \tag{10}$$

Then one can write the one-turn matrix including the beam–beam interactions:

$$M'_{i,j} = \prod_{l}^{N_{\text{BB}}} M_{i,l} M^{BB}_{i,j,l} \ , \tag{11}$$

with $M^{BB}_{i,j,l}$ the non-linear beam–beam map of beam i, bunch j at location l defined by

$$M^{BB}_{i,j,l} : x'_{i,j} \mapsto x'_{i,j} + \Delta x'_{\text{coh}}(x_{i,j} - x_{S(i,j,l)}) \ . \tag{12}$$

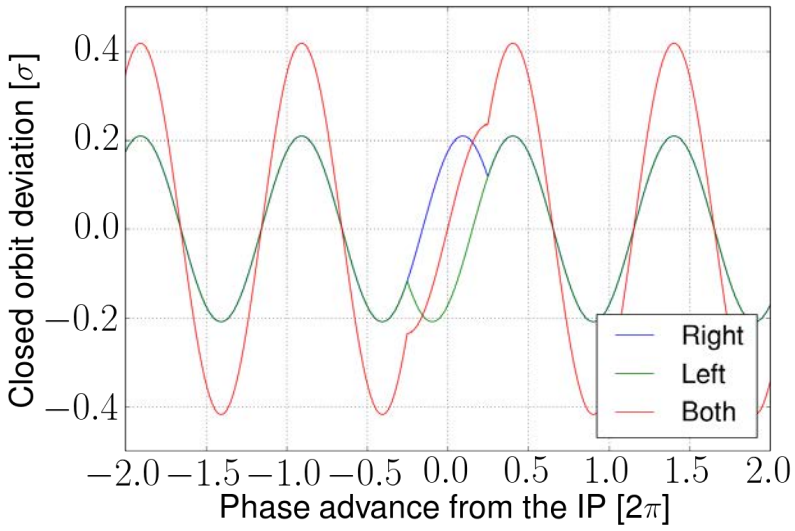

Fig. 2: Illustration of the orbit of three PACMAN bunches in an interaction region with a crossing angle around the interaction point. One experiences a long-range beam–beam interaction only on the left-hand side of the interaction point (green), the other only on the right-hand side (blue), and the last on both sides (red). While the common part of the orbit effect can be corrected using standard orbit correctors, a spread of the closed orbit remains.

The knowledge of the collision scheme was introduced with the function $S(i, j, l)$ giving the indices identifying the bunch of the other beam colliding with bunch j of beam i at the location l. In the absence of beam–beam interaction at the given location, the beam–beam map becomes the identity. Thus, the problem can be reformulated as a closed orbit problem:

$$\bar{x}_{i,j,k+1} = M'_{i,j} \cdot \bar{x}_{i,j,k} \ , \tag{13}$$

where the fixed point gives the closed orbit of the different bunches of each beam, see Ref. [6].

This effect was critical at the Large Electron–Position Collider (LEP), when operated with bunch trains. The orbit variations due to long-range beam–beam interactions resulted in a luminosity loss due to bunches colliding with an offset at the interaction point, see Ref. [7]. It is important to note that since different bunches have different orbits, any correction scheme needs to be fast enough to act differently on individual bunches. In the LHC, the orbit effect at the interaction point is much smaller than the beam size, and the effect on the luminosity is therefore negligible. A harmless displacement of the luminous region could be observed by the experiments (Fig. 3). While small, the orbit variations due to beam–beam interactions play an important role when performing Van Der Meer scans for luminosity calibration, see Ref. [8].

3.2 Dynamic β effect

The formalism developed in previous section to evaluate the bunch by bunch orbits can be extended, by including higher orders in the beam–beam map, in order to allow for the computation of the modification of the machine optics due to multiple head-on and long-range beam–beam interactions. Similarly, one finds that beam–beam interactions cause individual bunches to have different optics functions. These effects may have an important impact on the performance of a collider since bunches with different tunes or different chromaticities may behave very differently in terms of lifetime, for example. In the case of the LHC, mitigation techniques had to be implemented, see Ref. [10]. In some cases, the modification of the optics may rather be controlled in order to reduce the β function at the interaction point and therefore achieve a higher luminosity, see Ref. [11].

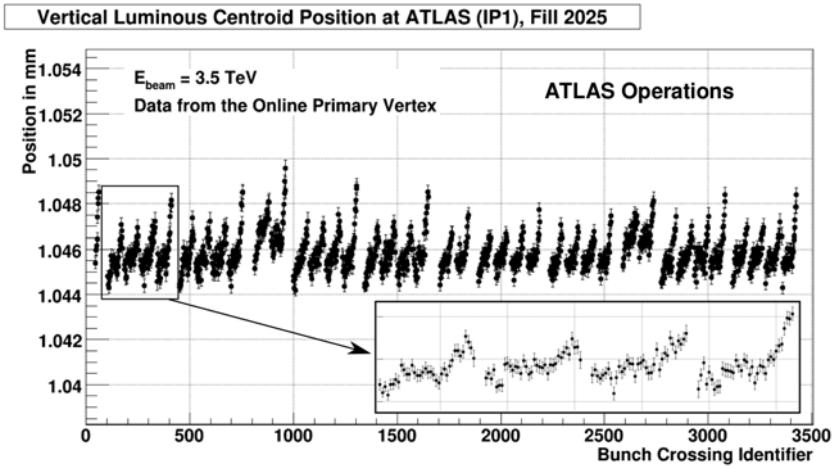

Fig. 3: Bunch-by-bunch displacement of the centroid of the luminous region measured by ATLAS during dedicated experiments in the LHC, see Ref. [9]. The correlation with the position of the bunch in the train, and consequently with the number of long-range beam–beam interactions, is clear.

While complex configurations of beam–beam interactions requires the use of a computer, one can derive equations to describe the dynamics in simpler, yet interesting, configurations. Let us consider a single head-on beam–beam interaction and approximate it to first order. The modification of the optics is then identical to the one due to a quadrupolar error Ref. [12]:

$$\left(\frac{\beta_0^*}{\beta^*}\right)^2 = 1 - \beta_0^* k_{\rm BB} \cot(2\pi Q_0) - \frac{1}{4}\beta_0^{*2} k_{\rm BB}^2 \,, \tag{14}$$

with β_0^* and β^* the unperturbed and perturbed β functions at the interaction point, and $k_{\rm BB}$ the quadrupolar strength of the head-on beam–beam interaction given by Ref. [2]

$$k_{\rm BB} = \frac{r_0 N}{\epsilon_n \beta^*} \,, \tag{15}$$

with ϵ_n the normalized transverse emittance. Assuming that both beams behave identically, we have

$$\left(\frac{\beta_0^*}{\beta^*}\right)^2 = 1 - 2ab\frac{\beta_0^*}{\beta^*} - \left(a\frac{\beta_0^*}{\beta^*}\right)^2 \,, \tag{16}$$

where we have introduced $a \equiv \dfrac{r_0 N}{2\epsilon_n}$ and $b \equiv \cot(2\pi Q_0)$ for convenience. The solution is then

$$\frac{\beta_0^*}{\beta^*} = -\frac{ab \pm \sqrt{1 + a^2(1+b^2)}}{1+a^2} \,. \tag{17}$$

Relaxing the assumption that the two beams have to behave identically, Eq. (14) becomes

$$\begin{cases} \left(\dfrac{\beta_0^*}{\beta_+^*}\right)^2 &= 1 - 2ab\dfrac{\beta_0^*}{\beta_-^*} - \left(a\dfrac{\beta_0^*}{\beta_-^*}\right)^2 \\ \left(\dfrac{\beta_0^*}{\beta_-^*}\right)^2 &= 1 - 2ab\dfrac{\beta_0^*}{\beta_+^*} - \left(a\dfrac{\beta_0^*}{\beta_+^*}\right)^2 \,, \end{cases} \tag{18}$$

where we have introduced β_+^* and β_-^* the β function of the two beams at the interaction point. The solutions given by Eq. (17) with $\beta_+^* = \beta_-^* = \beta^*$, remains a solution of the system, yet it admits two other solutions with $\beta_+^* \neq \beta_-^*$:

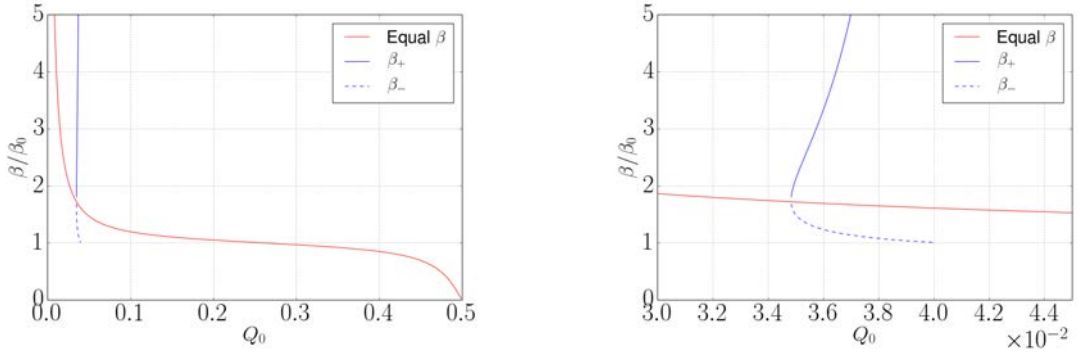

(a) **(b)** zoom

Fig. 4: Dynamic β effect for a beam–beam parameter of 0.02

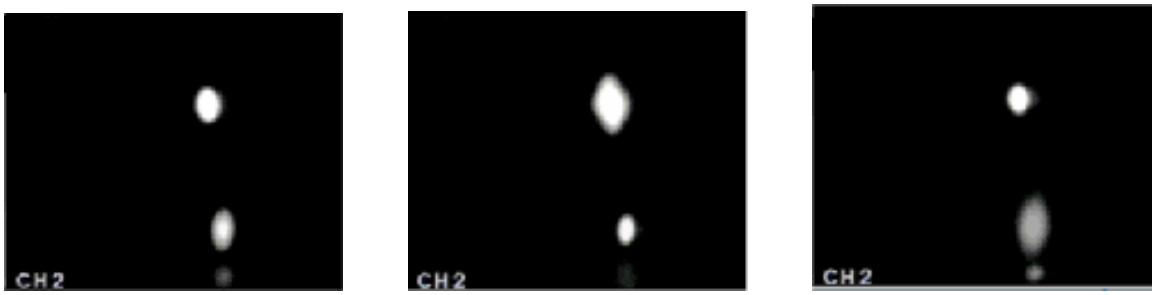

(a) Equal **(b)** Blown-up positron beam **(c)** Blown-up electron beam

Fig. 5: Flip–flop effect observed at VEPP-2000, see Ref. [13]. With small beam–beam parameters the two beams stay symmetric (left-hand side), but for $\xi \gtrapprox 0.1$ two asymmetric configurations are observed (right-hand side).

$$\frac{\beta_0^*}{\beta_\pm^*} = \frac{ab(1-a^4) \pm \sqrt{(a^2-1)^2(a^2+1)(1+a^4(1+b^2)-a^2(2+3b^2))}}{(a^2-1)^2(a^2+1)} \,. \tag{19}$$

The two solutions (Fig. 4) correspond to one of the two beams being blown-up, whereas the other is squeezed. Since the two beams are identical, both solutions are perfectly equivalent, yet the system may spontaneously chose one of the states, and possibly switch between the two under small perturbations, resulting in the so-called flip–flop effect (Fig. 5), see Refs. [13–15].

4 Coherent beam–beam modes

Assuming that a proper description of the new equilibrium condition including beam–beam interactions was found, we study the oscillation of the two beams around that equilibrium. In the weak–strong regime, the two beams oscillate independently of each other, but in strong–strong configurations the two beams may oscillate coherently. The strong–strong condition is, however, not sufficient to ensure coherent oscillation of the two beams, several mechanisms of decoherence exists. This section introduces the different models used to describe the coherent modes of oscillation and their decoherence.

4.1 Models

4.1.1 The rigid-bunch model

A first step in the description of the coherent beam–beam modes consists in solving the equations of motion of the two beams self-consistently, allowing for their respective transverse positions and momentum

to vary, while all other parameters are kept constant. In other words, the beam distributions are fixed to the equilibrium one, usually assumed to be Gaussian. The two beams are then modelled by their average position and momentum (x_i, x_i'), with respect to their closed orbits. We follow an approach similar to the one developed in Section 3 to derive the one-turn map including self-consistently the beam–beam interactions. Since we are interested in small amplitude modes of oscillations, we keep only the first-order terms, the maps therefore becoming matrices. The normal-mode analysis of the one-turn matrix, including the beam–beam interactions self-consistently, will provide the coherent mode of oscillation. Let us start with the one-turn matrix of each beam:

$$\begin{pmatrix} x_{i,k+1} \\ x'_{i,k+1} \end{pmatrix} = \begin{pmatrix} \cos(2\pi Q) & \beta \sin(2\pi Q) \\ -\dfrac{1}{\beta}\sin(2\pi Q) & \cos(2\pi Q) \end{pmatrix} \cdot \begin{pmatrix} x_{i,k} \\ x'_{i,k} \end{pmatrix} . \tag{20}$$

For the two identical beams, we have (see Eq. (8))

$$\begin{pmatrix} x_{1,k+1} \\ x'_{1,k+1} \\ x_{2,k+1} \\ x'_{2,k+1} \end{pmatrix} = \begin{pmatrix} \cos(2\pi Q) & \beta \sin(2\pi Q) & 0 & 0 \\ -\dfrac{1}{\beta}\sin(2\pi Q) & \cos(2\pi Q) & 0 & 0 \\ 0 & 0 & \cos(2\pi Q) & \beta \sin(2\pi Q) \\ 0 & 0 & -\dfrac{1}{\beta}\sin(2\pi Q) & \cos(2\pi Q) \end{pmatrix} \cdot \begin{pmatrix} x_{1,k} \\ x'_{1,k} \\ x_{2,k} \\ x'_{2,k} \end{pmatrix} \equiv M_0 \cdot \begin{pmatrix} x_{1,k} \\ x'_{1,k} \\ x_{2,k} \\ x'_{2,k} \end{pmatrix} , \tag{21}$$

where we have defined M_0 as the two-beam one-turn matrix. The matrix for a beam–beam interaction may be derived by linearizing Eq. (3) around (x_0, y_0), the closed orbit difference between the two beams at the interaction point:

$$\Delta x'_{\text{coh}}(x, y) \approx \Delta x'_{\text{coh}}(x_0, y_0) + \frac{\partial \Delta x'_{\text{coh}}}{\partial x}(x_0, y_0)\Delta x \, , \tag{22}$$

with

$$\frac{\partial \Delta x'_{\text{coh}}}{\partial x}(x, y) = -\frac{2Nr_0}{\gamma_r}\left[\left(\frac{1}{r^2} - \frac{x^2}{r^4}\right)\left(1 - \mathrm{e}^{-\dfrac{-r^2}{4\sigma^2}}\right) + \frac{x^2}{2r^2\sigma^2}\mathrm{e}^{-\dfrac{-r^2}{4\sigma^2}}\right] . \tag{23}$$

Defining $k_0 \equiv \dfrac{\partial \Delta x'_{\text{coh}}}{\partial x}(x_0, y_0)$, one can then write the coupling matrix between the two beams, due to the beam–beam interaction:

$$M_{\text{BB}} = \begin{pmatrix} 1 & 0 & 0 & 0 \\ -k_0 & 1 & k_0 & 0 \\ 0 & 0 & 1 & 0 \\ k_0 & 0 & -k_0 & 1 \end{pmatrix} . \tag{24}$$

Thus we can write the one-turn matrix of the two beams including a single beam–beam interaction:

$$\begin{pmatrix} x_{1,k+1} \\ x'_{1,k+1} \\ x_{2,k+1} \\ x'_{2,k+1} \end{pmatrix} = M_{\text{BB}} \cdot M_0 \cdot \begin{pmatrix} x_{1,k} \\ x'_{1,k} \\ x_{2,k} \\ x'_{2,k} \end{pmatrix} . \tag{25}$$

The normal-mode analysis reveals two frequencies each corresponding to two degenerated modes. The first mode corresponds to in-phase oscillation of the two beams (σ-mode), and its coherent tune is the unperturbed machine tune $Q_\sigma = Q$. The second mode of oscillation corresponds to out-of-phase oscillation of the two beams (π-mode); we have

$$\cos(2\pi Q_\pi) = \cos(2\pi Q) - \beta^* k_0 \sin(2\pi Q) \, . \tag{26}$$

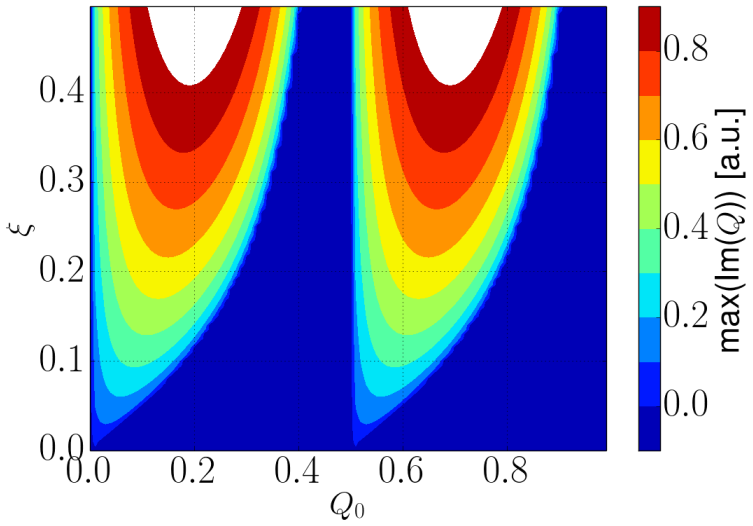

Fig. 6: Largest imaginary part of the eigenvalues of Eq. (25), defining the stable area in terms of unperturbed tune Q_0 and beam–beam parameter ξ.

The stability of the beam–beam modes is given by the imaginary part of the eigenvalues of the matrix given by Eq. (25), which is reported in Fig. 6. From a comparison with Eq. (26), we see that the stability boundary is given by the resonance condition $2Q_\pi = n$. Since we have limited our description of the lattice and of the beam–beam interactions to first order, only the lowest-order resonance are visible. In principle higher-order resonances could also drive the coherent beam–beam modes, see Ref. [16]. It is therefore important to make sure there exist damping mechanisms for these modes; the description of these mechanisms requires more powerful models.

4.1.2 Vlasov perturbation theory

While the rigid-bunch model provides a reasonable description of the coherent modes, the non-linearity of the beam–beam force is neglected. In order to fully assess the effect of the non-linearities on the coherent motion of the two beams, we start from the Liouville equation for the two beams' distributions $\Psi_{1,2}$ with their respective Hamiltonians H_1 and H_2:

$$\begin{cases} \dfrac{\partial \Psi_1}{\partial t} &= \{H_1, \Psi_1\} \\ \\ \dfrac{\partial \Psi_2}{\partial t} &= \{H_2, \Psi_2\} \ , \end{cases} \tag{27}$$

with $\{\cdot, \cdot\}$ denoting the Poisson brackets. The equations are coupled, since the Hamiltonian for a given beam depends on the electromagnetic field generated by the other beam and consequently on its distribution. While mathematically more involved, the treatment of this system of equations is similar to the approach taken in the rigid-bunch approximation. Having derived a Hamiltonian describing both the lattice and the beam–beam interactions, the system can be linearized around the equilibrium distribution $\Psi_{i,0}$ by introducing a first-order perturbation of the distribution $\Psi_i = \Psi_{i,0} + \Psi_{i,1}$. The modes of oscillation and their frequencies are then obtained through the normal-mode analysis of the corresponding linear operator, see Refs. [17, 18]. While the rigid-bunch model only considers fixed particle distributions, the perturbation $\Psi_{i,1}$ is properly matched to the non-linear system. As a result, the frequency of the coherent modes of oscillation is modified. Away from resonances, Eq. (26) obtained within the

rigid-bunch model can be approximated by

$$Q_\pi = Q_0 - \xi \,, \tag{28}$$

while within Vlasov perturbation theory, the frequency shift of the π-mode with respect to the unperturbed tune is increased by the so-called Yokoya factor Y:

$$Q_\pi = Q_0 - Y\xi \,. \tag{29}$$

The values of the Yokoya factor depends on the geometry of the beam–beam interaction, e.g. for round beams ($\sigma_x = \sigma_y$) we have $Y \approx 1.21$ and $Y \approx 1.33$ for flat beams ($\sigma_x \gg \sigma_y$), see Ref. [17]. This model has been shown to provide the most accurate value of the frequency of the coherent beam–beam mode in several colliders Refs. [19–22].This frequency shift has an important impact on the stability of the coherent beam–beam modes. We shall discuss further this aspect in Section 4.2. Let us first consider the limitations of the present model. We approximate the perturbation to first order, i.e neglecting high-order terms of the beam–beam interactions, which has a small impact on the prediction of the modes frequencies. These higher-order terms might, however, impact significantly on the stability of the coherent modes, e.g. through Landau damping. Also, one may note that an accurate description of the interplay between the effect of beam–beam interactions and other mechanisms such as lattice-induced non-linearities or the beam-coupling impedance becomes very cumbersome in this formalism.

4.1.3 Multiparticle tracking simulations

The use of computer tracking simulations allows for an accurate description of the coherent dynamics of the two beams in arbitrarily complex configurations of beam–beam interactions. The interplay with other mechanisms is also conveniently described using a modular description of the different effect as in Ref. [23]. Also, strong assumptions can be relaxed with respect to most theoretical approaches, the cost being in computational resources. Similarly to the method described in Ref. [23], we model the two beams by a set of charged macro-particles. The effect of beam–beam interactions is introduced by evaluating the electromagnetic fields generated by the distribution of macro-particles and apply the corresponding variation of the macro-particles' momentum of the other beam. In cases where the equilibrium particle distribution is close to Gaussian, the fields can be computed based on the numerical evaluation of the moments of the other beam's particle distribution, using the analytical formula for the beam–beam kick (see Eq. (1)). This so-called soft-Gaussian approximation has the advantages of being computationally cheap and introduces a minimal amount of numerical noise in the simulation. In high-energy lepton colliders, the equilibrium distribution is far from Gaussian, due to the effect of synchrotron radiation and the non-linearities of the beam–beam interactions. The use of the soft-Gaussian approximation is therefore excluded in these cases, see Ref. [24]. Numerical solvers for the Poisson equation should be used instead, resulting in fully self-consistent simulations of the beam–beam interactions. Let us illustrate the impact of the different approximations by simulating the simple configuration analysed in previous section, i.e. two bunches colliding in a single interaction point. The Fourier transform of the turn-by-turn position of one of the beam is shown in Fig. 7 for two simulations using either the soft-Gaussian approximation or a fully self-consistent calculation using the HFMM algorithm, see Ref. [25]. One observes that the soft-Gaussian method provides a better estimate of the π-mode frequency with respect to the rigid-bunch model; it is, however, not accurate enough to provide the same frequency as provided by the Vlasov perturbation theory.

Coherent beam-beam modes were observed in most colliders with frequencies in remarkable agreement with the predictions of both Vlasov perturbation theory and tracking simulations. An example of such observation in the LHC is shown in Fig. 8.

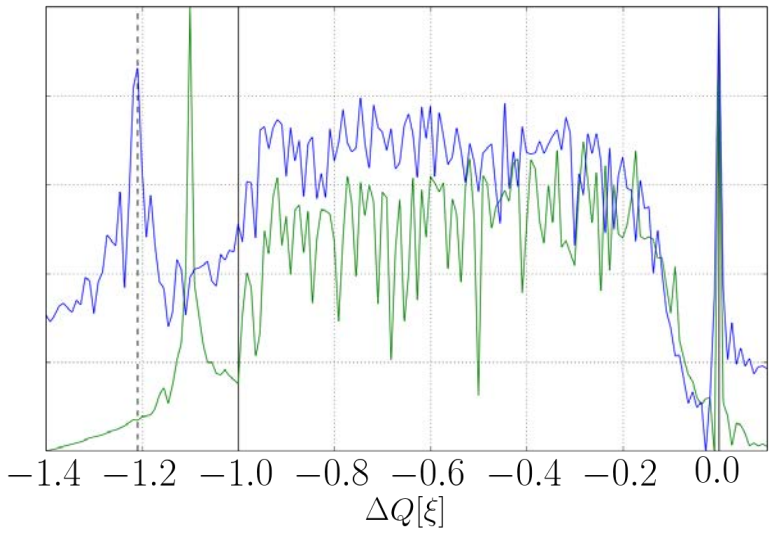

Fig. 7: Comparison of the spectrum obtained with tracking simulation of two bunches colliding in a single interaction point with different models for the beam–beam interactions. The solid black lines show the predictions of the rigid-bunch model, while the dashed black line corresponds to the Vlasov perturbation theory. The green and blue lines correspond to tracking simulations using respectively the soft-Gaussian approximation and a fully self-consistent model.

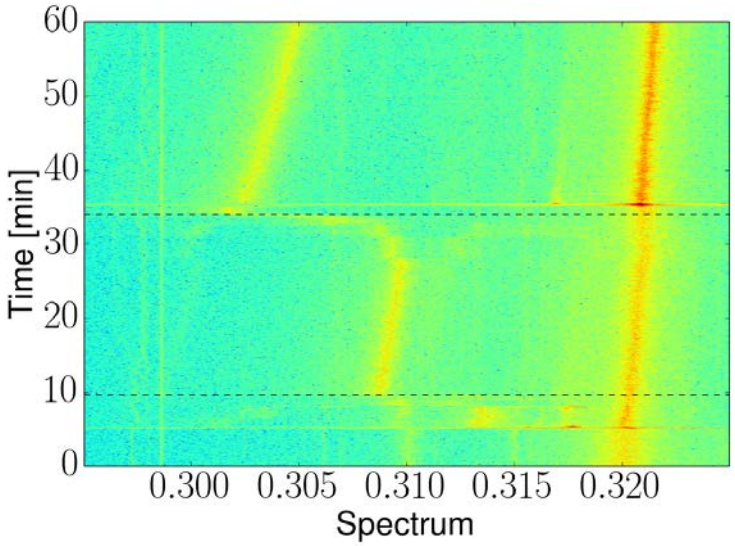

Fig. 8: Measured spectrogram during a dedicated experiment at the LHC with a single bunch per beam. The first dashed line indicates when the beams were brought into collision in one interaction point, revealing a second line shifted down with respect to the unperturbed tune $Q \approx 0.32$ corresponding to the beam–beam π-mode. The second dashed line indicates when the second interaction point is put into collision, pushing the frequency of the beam–beam π-mode further down.

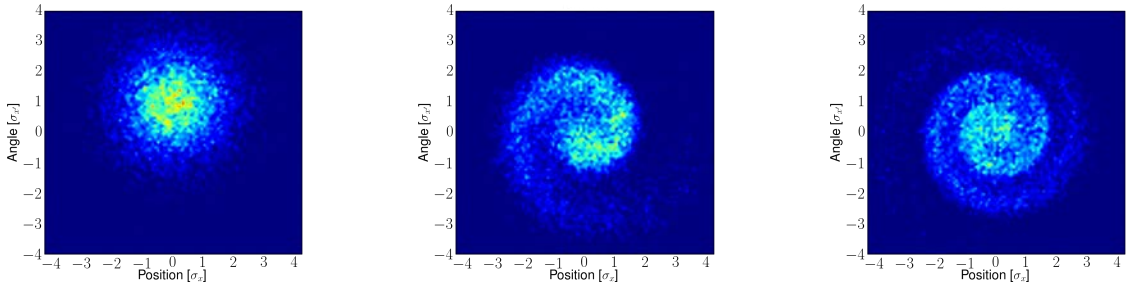

(a) Turn 1 **(b)** Turn 400 **(c)** Turn 800

Fig. 9: Evolution of the transverse phase-space density of a beam under the influence of a beam–beam interaction in the weak strong regime. The initial coherent kick equal to the beam divergence σ'_x decoheres rapidly due to the spread in the oscillation frequency of the individual particles.

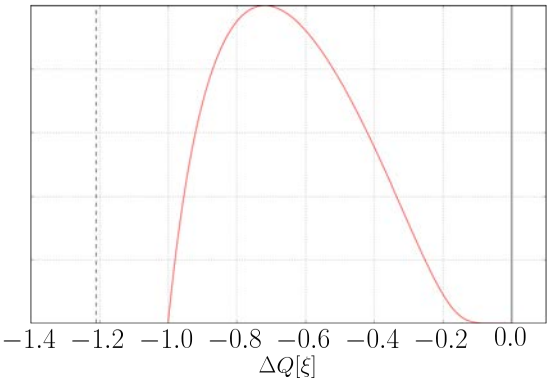

Fig. 10: Spectrum of the single-particle frequencies (red), compared with the frequencies of the coherent modes of oscillation (solid black: σ-mode, dashed black: π-mode) for two symmetric round beams colliding head-on in a single interaction point.

4.2 Decoherence and Landau damping

The presence of external sources of noise acting on the beam, e.g. due to the ripple of dipole fields, leads to emittance growth through filamentation, see Ref. [26]. This effect is illustrated in Fig. 9. In the weak–strong regime, the effect of beam–beam interactions can be treated similarly to other lattice non-linearities, see Ref. [27]. In particular, the motions of the single particles are regular, but the frequency spread results in a damping of the coherent motion at the cost of an increase of the beam emittance. In the presence of beam–beam interactions in the strong–strong regime, the situation is very different. Although the model described in Section 4.1.2 allows for a consistent treatment of decoherence and Landau damping, see Ref. [18], here we rather use a simpler model in order to illustrate the mechanism. The main difference with respect to the filamentation mechanism in the weak–strong regime is the presence of a gap between the coherent-mode frequencies and the single-particle frequencies. This can be understood by considering the equation of motion of a single particle, in the presence of an external force dependent on the single-particle position x_i and on the position of the bunch centroid $\langle x \rangle$, $F(x_i, \langle x \rangle)$:

$$\ddot{x}_i + \omega_0 x_i = \frac{F(x_i - \langle x \rangle)}{m} \,, \tag{30}$$

where $\omega_0 = 2\pi Q$ is the unperturbed tune. In the weak–strong regime, the position of the bunch centroid is fixed, let us chose $\langle x \rangle = 0$ meaning head-on collision of the two beams. Following Ref. [2], we can

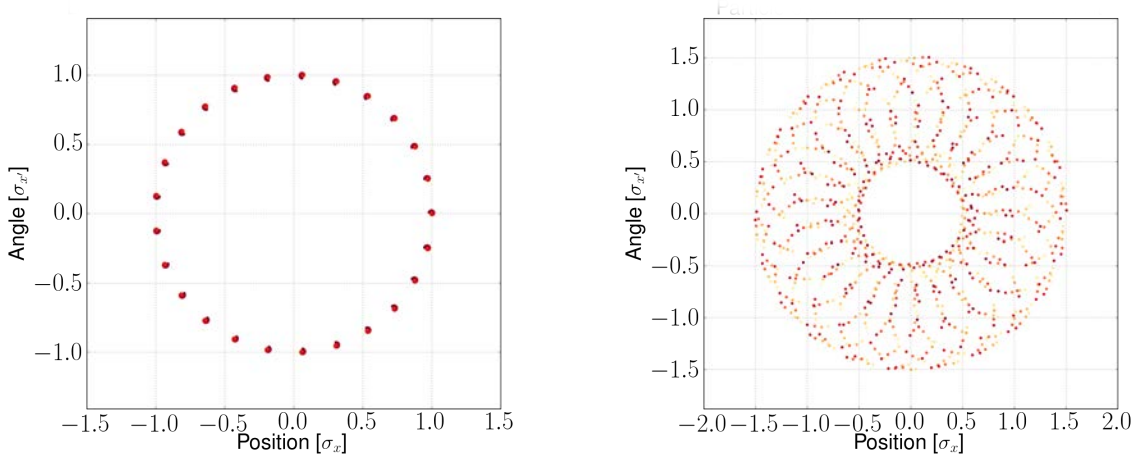

(a) Centroid motion

(b) Single-particle motion

Fig. 11: Evolution of a single particle and of the beam centroid position in a fully self-consistent simulation of two symmetric beams colliding head-on. In this configuration, the coherent modes are outside of the incoherent spectrum (Fig. 10), and the absence of decoherence is clearly visible, since the amplitude of oscillation of the centroid position remains constant over time. The single-particle motion is a composition of the incoherent motion and the driven oscillation at the frequency of the beam–beam mode.

write

$$\ddot{x}_i + \omega_i x_i = 0 \,, \tag{31}$$

where ω_i is the perturbed frequency of oscillation of the particle i. Since the perturbed frequency depends on the amplitude of oscillation, the different oscillation amplitudes in the beam results in a frequency distribution, which is represented in Fig. 10 for the particular case of two Gaussian beams colliding head-on. Let us now assume that the two beams oscillate coherently with an amplitude A at a frequency $\Omega = 2\pi Q$. The average position of the beams becomes

$$\langle x_i \rangle = A \cos(\Omega t) \,. \tag{32}$$

The external force becomes time dependent; following the same procedure, Eq. (30) becomes

$$\ddot{x}_i + \omega_0 x_i = \frac{F(x_i - A\cos(\Omega t))}{m} \,. \tag{33}$$

Approximating the external force to first order, we have

$$\ddot{x}_i + \omega x_i = \frac{1}{m}\frac{\partial F(0)}{\partial x} A \cos(\Omega t) \,, \tag{34}$$

which is the equation of a driven oscillator, and the solution for the single-particle motion with $\omega \neq \Omega$ is given by

$$x_i(t) = A_i \cos(\omega_i t + \phi_i) + A_{\mathrm{coh},i} \cos(\Omega t). \tag{35}$$

While A_i and ϕ_i are determined by the initial conditions of each single particles, A_{coh} is given by

$$A_{\mathrm{coh},i} = \frac{1}{m}\frac{\dfrac{\partial F(0)}{\partial x} A}{\omega_i^2 - \Omega^2} \,. \tag{36}$$

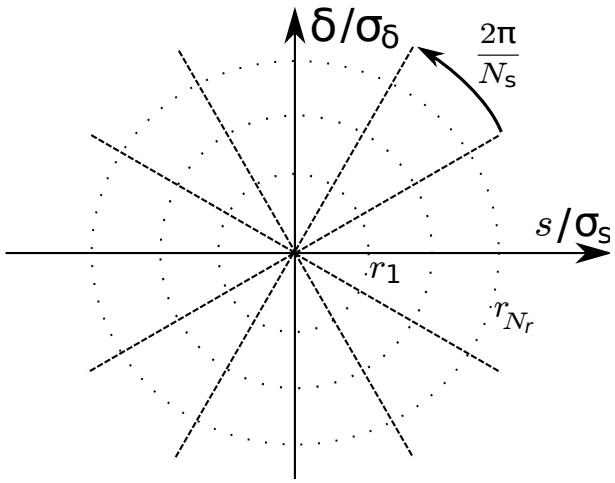

Fig. 12: Discretization of the longitudinal phase space into N_s slices and N_r rings

The bunch centroid position is obtained by averaging Eq. (35) over the particles. Since the initial distribution of phases is assumed uniform, the first term averages out, while the second term remain, we have

$$\langle x_i \rangle(t) = \langle A_{\mathrm{coh},i} \rangle \cos(\Omega t) \; . \tag{37}$$

The exact value of the single-particle amplitudes is not easily obtained within this model, since the excitation amplitude (see Eq. (32)) and the average over all particles (see Eq. (37)) need to be treated consistently. Yet this model shows an important feature of the coherent excitation: its oscillatory component persists, or in other words there is no mechanism of decoherence in these conditions. This effect is illustrated with fully self-consistent macro-particle simulations in Fig. 11. The single-particle motion is well described by the combination of its oscillation at its frequency ω_i and the forced oscillation at frequency of the coherent mode Ω. The oscillation of the bunch centroid around the closed orbit is, however, unperturbed by the presence of the frequency spread as opposed to the result obtained in the weak–strong regime (Fig. 9).

The presence of a resonant condition between the coherent motion and single particles $\omega_i = \Omega$ leads to divergence of the amplitude of oscillation of the single particles (see Eq. (36)), which suggests that there is an energy transfer between the coherent force and the resonant single particles and therefore indicates a decoherence mechanisms. In other words, the necessary condition for damping of the coherent modes is the presence of an overlap between the single-particle frequency spread and the coherent-mode frequency.

While this analysis illustrates the importance of the strong–strong treatment in the understanding of decoherence, more powerful models based on Vlasov equation are needed to properly describe both decoherence and Landau damping in such conditions, see Ref. [18, 28].

4.3 Beam coupling impedance

The impact of beam–beam interactions on the stability of impedance-driven modes is twofold. In the weak–strong regime, the frequency spread resulting from the non-linearities of the beam–beam forces have an impact on the Landau damping of the head-tail modes, which can be quantified using their dispersion relation, see Refs. [2, 28]. If the two beams oscillate coherently, the modes of oscillation are different with respect to the single-beam modes, and therefore they do not satisfy the same dispersion relation. A model describing both the effect of the beam coupling impedance and of the beam–beam interactions is necessary to assess the stability of the coherent beam–beam modes under the influence of the beam coupling impedance. The circulant matrix model, see Refs. [29–31], offers a convenient way

to describe the transverse oscillation of the beams, including the effect of the transverse wake fields and beam–beam interactions. This model is an extension of the rigid-bunch model, allowing for different part of the longitudinal phase space to oscillate independently. The longitudinal phase space is discretized in polar coordinates into so-called slices and rings as illustrated in Fig. 12. The transverse motion of each discrete element can be treated as in the rigid-bunch model, except that all the combinations of beam–beam interactions between the elements need to be considered. Equation 22 becomes

$$\Delta x_i = k_0 \left(\frac{\sum_{j=0}^{N_s N_r} Q_j x_j}{\sum_{j=0}^{N_s N_r} Q_j} - x_i \right) . \tag{38}$$

As an example, let us use two slices and a single ring, and start from Eq. (25):

$$\begin{pmatrix} x_{1,1,k+1} \\ x'_{1,1,k+1} \\ x_{1,2,k+1} \\ x'_{1,2,k+1} \\ x_{2,1,k+1} \\ x'_{2,1,k+1} \\ x_{2,2,k+1} \\ x'_{2,2,k+1} \end{pmatrix} = M_{\text{BB}} \cdot M_0 \cdot \begin{pmatrix} x_{1,1,k} \\ x'_{1,1,k} \\ x_{1,2,k} \\ x'_{1,2,k} \\ x_{2,1,k} \\ x'_{2,1,k} \\ x_{2,2,k} \\ x'_{2,2,k} \end{pmatrix} , \tag{39}$$

where $x_{i,j,k}$ refer to the position of slice j from beam i at turn k. The lattice matrix M_0 can easily be extended, since all slices go through the same lattice, and the beam–beam coupling matrix becomes

$$M_{\text{BB}} = \begin{pmatrix} 1 & 0 & 0 & 0 & 0 & 0 & 0 & 0 \\ -k_0 & 1 & 0 & 0 & k_0/2 & 0 & k_0/2 & 0 \\ 0 & 0 & 1 & 0 & 0 & 0 & 0 & 0 \\ 0 & 0 & -k_0 & 1 & k_0/2 & 0 & k_0/2 & 0 \\ 0 & 0 & 0 & 0 & 1 & 0 & 0 & 0 \\ k_0/2 & 0 & k_0/2 & 0 & -k_0 & 1 & 0 & 0 \\ 0 & 0 & 0 & 0 & 0 & 0 & 1 & 0 \\ k_0/2 & 0 & k_0/2 & 0 & 0 & 0 & -k_0 & 1 \end{pmatrix} . \tag{40}$$

Such a matrix can be build in a systematic way for an arbitrary number of slices an rings, and, for a complex configuration of beam–beam interactions, following the same approach as in Section 3.1, see Ref. [32]. In order to introduce the effect of the wake, we need to take a closer look at the discretization of the longitudinal phase space. In particular, the longitudinal position of the discrete elements needs to be defined. The definition of the discretization is somewhat arbitrary, but it is convenient to split the phase space such that the charge contained in each element is identical, as was implicitly assumed when deriving Eq. (40). For a Gaussian distribution of particles, the slices are uniformly distributed $\theta_i = 2\pi i / N_s$ and the radius of the rings set such that

$$\mathrm{e}^{-r_{j+1}} - \mathrm{e}^{-r_j} = \frac{1}{N_r} , \tag{41}$$

where $r_j = \sqrt{(s_j/\sigma_s)^2 + (\delta_j/\sigma_\delta)^2}$ is the radius of the jth ring in the normalized longitudinal phase space, i.e. σ_s and σ_δ are the bunch length and relative momentum spread. Therefore one obtains the longitudinal position $s_{i,j}$ and moment deviations $\delta_{i,j}$ of the ith slice and jth ring:

$$\begin{cases} s_{i,j} &= r_j \sigma_s \cos\theta_i \\ \delta_{i,j} &= r_j \sigma_\delta \sin\theta_i \, . \end{cases} \tag{42}$$

Thus we can write the interaction between the discrete elements of the distribution through the beam coupling by using the integrated dipolar and quadrupolar wake functions $W_{\text{dip}}(\Delta s)$ and $W_{\text{quad}}(\Delta s)$, see Ref. [33]:

$$\Delta x_i' = \sum_{j=0}^{N_s N_r} W_{\text{dip}}(s_j - s_i)x_j + W_{\text{quad}}(s_j - s_i)x_i \; . \tag{43}$$

This can be written in a matrix form, in our two-slice model and assuming that the two beams experience identical impedances, we have

$$M_{\text{Z}} = \begin{pmatrix} 1 & 0 & 0 & 0 & 0 & 0 & 0 & 0 \\ W_{\text{quad}}(s_1 - s_0) & 1 & W_{\text{dip}}(s_1 - s_0) & 0 & 0 & 0 & 0 & 0 \\ 0 & 0 & 1 & 0 & 0 & 0 & 0 & 0 \\ W_{\text{dip}}(s_0 - s_1) & 0 & W_{\text{quad}}(s_0 - s_1) & 1 & 0 & 0 & 0 & 0 \\ 0 & 0 & 0 & 0 & 1 & 0 & 0 & 0 \\ 0 & 0 & 0 & 0 & W_{\text{quad}}(s_1 - s_0) & 1 & W_{\text{dip}}(s_1 - s_0) & 0 \\ 0 & 0 & 0 & 0 & 0 & 0 & 1 & 0 \\ 0 & 0 & 0 & 0 & W_{\text{dip}}(s_0 - s_1) & 0 & W_{\text{quad}}(s_0 - s_1) & 1 \end{pmatrix} , \tag{44}$$

such that the equation of motion becomes

$$\begin{pmatrix} x_{1,1,k+1} \\ x'_{1,1,k+1} \\ x_{1,2,k+1} \\ x'_{1,2,k+1} \\ x_{2,1,k+1} \\ x'_{2,1,k+1} \\ x_{2,2,k+1} \\ x'_{2,2,k+1} \end{pmatrix} = M_{\text{Z}} \cdot M_{\text{BB}} \cdot M_0 \cdot \begin{pmatrix} x_{1,1,k} \\ x'_{1,1,k} \\ x_{1,2,k} \\ x'_{1,2,k} \\ x_{2,1,k} \\ x'_{2,1,k} \\ x_{2,2,k} \\ x'_{2,2,k} \end{pmatrix} \; . \tag{45}$$

We have written the transverse one-turn matrix for the longitudinal distribution, yet the longitudinal motion has been put aside. Thanks to the choice of decomposition of the longitudinal phase space, the longitudinal motion can be introduced rather simply, as it consists of a rotation of the slices. The longitudinal one-turn matrix is given by the circulant matrix

$$S_r = P_{N_{\text{s}}}^{N_{\text{s}} Q_s} \; , \tag{46}$$

where Q_s is the synchrotron tune and $P_{N_{\text{s}}}$ is a permutation matrix,

$$P_{N_{\text{s}}} = \begin{pmatrix} 0 & 1 & & & \\ & 0 & 1 & & \\ & & \ddots & \ddots & \\ 1 & & & 0 & 1 \end{pmatrix} \; . \tag{47}$$

Since the rotation is identical for all rings and for both beams, the matrix in the same basis can be built using the outer product with identity matrix:

$$M_s = \mathbb{I}_2 \otimes \mathbb{I}_{N_{\text{r}}} \otimes S_r \otimes \mathbb{I}_2 \; . \tag{48}$$

The full one-turn matrix, including the synchro-betatron motion, the beam coupling and beam–beam interactions is then given by

$$M = M_{\text{Z}} \cdot M_{\text{BB}} \cdot M_s \cdot M_0 \; , \tag{49}$$

and its stability can be studied through normal-mode analysis. Let us discuss a simple configuration of two identical bunches colliding at a single interaction point, assuming that the lattice and the impedance

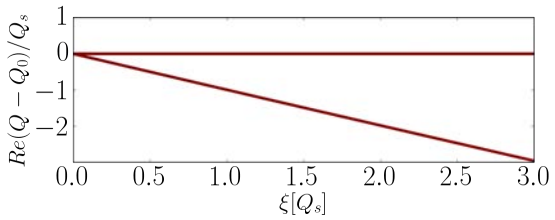

(a) 1 ring, 1 slice

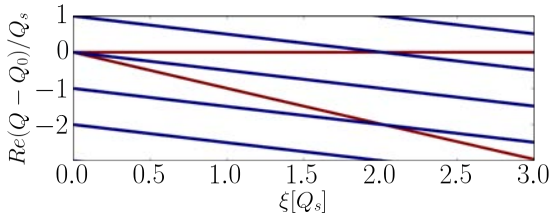

(b) 1 ring, 10 slices

Fig. 13: Eigenfrequencies of the coherent mode of oscillation of two round symmetric beams colliding head-on in on single interaction point for different beam–beam parameter. The points are colour coded according to their dipole moment: the σ and π modes are purely dipolar (red), while the synchrotron sidebands have no dipolar moment (blue). The eigenvalues are all real in the absence of other mechanisms.

experienced by both beams are identical. Figure 13(a) shows the frequency of the two normal modes obtained with a single slice and a single ring. As expected, we obtain the same solution as the rigid-bunch model, where the σ-mode frequency stays unperturbed, while the π-mode frequency is shifted by $-\xi$. Figure 13(b) shows the same result with a single ring and 10 slices, which allows us to see the frequency of azimuthal modes, appearing as sidebands of the betatron tune. Their frequencies are shifted by $-\xi/2$ due to the beam–beam interaction. This difference between the behaviour of the sidebands can be understood by looking at Eq. (38), where we observe that the sum over the positions of the slices is actually the dipolar moment of the oscillation. Since only the azimuthal mode 0 has a dipolar component, the other modes are only affected by the beam–beam interaction in an incoherent way. In other words, the frequency of the modes are shifted, but the corresponding sidebands of the two beams do not oscillate coherently. In the presence of wake fields the situation is different, since the perturbed azimuthal modes may also have a dipolar component. Figure 14(a) illustrates the impact of a resistive wall impedance on the frequency of the normal mode in the same configuration. The perturbed modes have indeed acquired a dipolar moment, which allows them to interact through the beam–beam interaction. This effect manifests strongly as a mode-coupling instability where the frequency of the π-mode reaches the one of the azimuthal mode -1 and where the frequency of the azimuthal mode 1 reaches the one of the σ-mode. Such an instability mechanism was observed in the LHC, see Ref. [31]. While the operation of the machine is not directly limited by these instabilities, passive or active mitigation techniques need to be put in place, e.g. adjusting the chromaticity or using a transverse feedback.

5 Complex configurations of beam–beam interactions

The complexity of the coherent beam–beam modes increases rapidly when considering realistic machines. In particular, the presence of multiple beam–beam interaction, both head-on or long-range, with different phase advances between the interactions and possibly asymmetries between the beams, create a variety of modes with different frequencies. To illustrate this complexity, the example of the nominal LHC is shown in Fig. 15. The computational power required to accurately describe such a complex system becomes important, even using the simplest models, see Ref. [34]. Let us illustrate the importance of such mechanisms with a simple example.

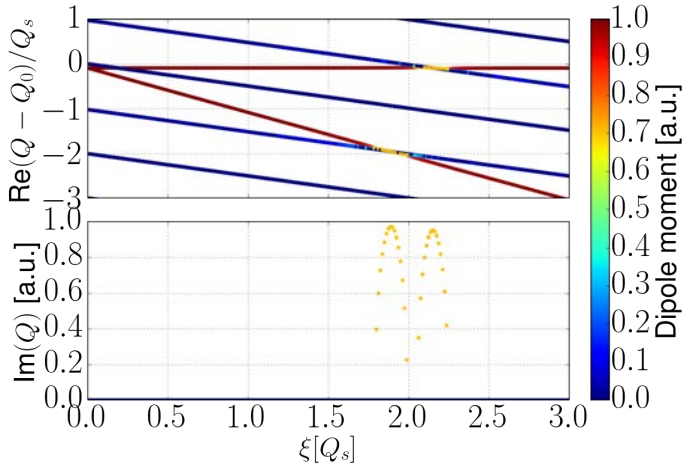

(a) $Q' = 0$

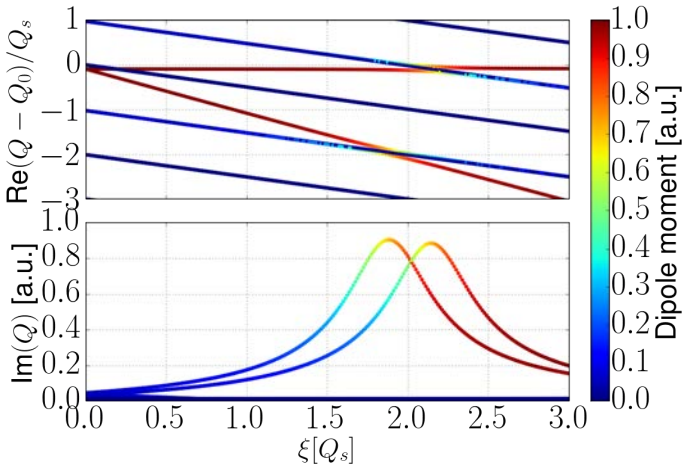

(b) $Q' = 2$

Fig. 14: Eigenfrequencies of the coherent mode of oscillation of two round symmetric beams colliding head-on in on single interaction point for different beam–beam parameter in the presence of a resistive-wall type of impedance. In the absence of chromaticity, a coupling instability appears when the frequencies of the coherent beam–beam modes reaches those of the synchrotron sidebands. In the presence of chromaticity, the coherent interaction between the two beams has an impact on the stability of head-tail modes, at any beam–beam parameters.

5.1 Tune split

Considering two beams with different unperturbed tunes Q_1 and Q_2 colliding in a single interaction point, we find the frequencies of the coherent mode of oscillation by diagonalizing the matrix of Eq. (25), with the one-turn matrix for the two beams:

$$M_0 = \begin{pmatrix} \cos(2\pi Q_1) & \beta\sin(2\pi Q_1) & 0 & 0 \\ -\frac{1}{\beta}\sin(2\pi Q_1) & \cos(2\pi Q_1) & 0 & 0 \\ 0 & 0 & \cos(2\pi Q_2) & \beta\sin(2\pi Q_2) \\ 0 & 0 & -\frac{1}{\beta}\sin(2\pi Q_2) & \cos(2\pi Q_2) \end{pmatrix} . \tag{50}$$

Figure 16 shows the behaviour of the frequencies when varying the tune split $\Delta Q = |Q_1 - Q_2|$. With $\Delta Q = 0$, we have the configuration studied previously, and the modes are outside the incoherent spectrum. However, for tune splits larger than the beam–beam parameter, the beams are decoupled and the

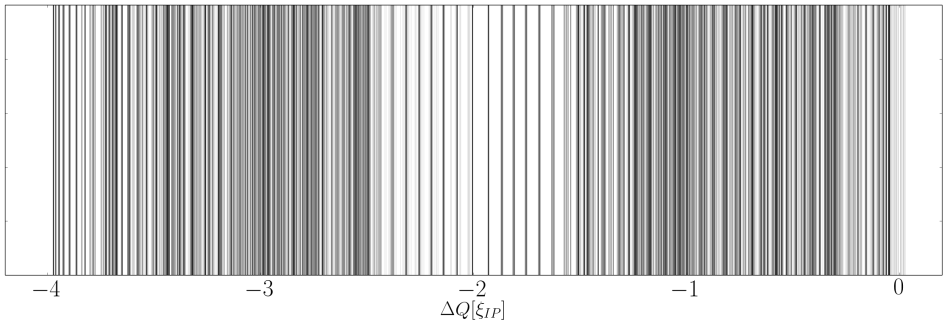

Fig. 15: The LHC coherent beam–beam mode pattern. Since each LHC beam is composed of 2808 bunches each experiencing a different pattern of head-on and long-range interactions, there are 2808^2 modes with different frequencies. The frequency is given in terms of the head-on tune shift per head-on interaction ξ_{IP}. Since there are up to four head-on interactions per bunch, the coherent-mode frequencies are spread between the unperturbed tune Q and $Q - 4\xi_{IP}$.

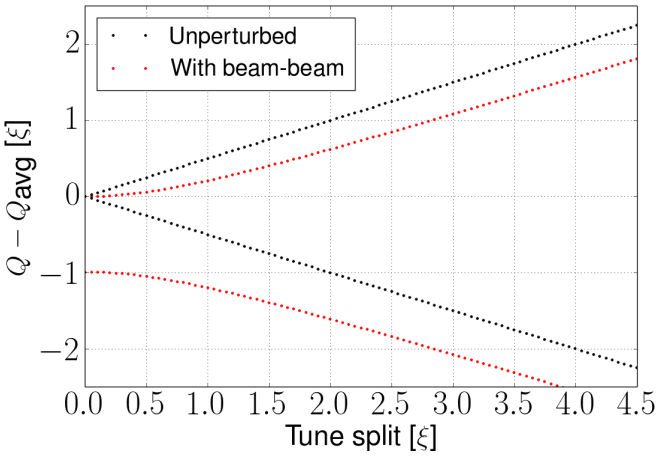

Fig. 16: Frequency of the coherent beam–beam modes for two beams with different tunes

frequency shift tends to half of the beam–beam parameter, i.e. the modes are brought back into the incoherent spectrum. In fact, since the two beams are decoupled because of their different frequencies, their behaviour becomes identical to the one derived for a weak–strong configuration.

References

[1] G. Franchetti, Space charge in circular machines, these proceedings.

[2] T. Pieloni, Beam–beam effects in hadron colliders, these proceedings.

[3] M. Bassetti and G. A. Erskine, Closed expression for the electrical field of a two-dimensional Gaussian charge, CERN-ISR-TH-80-06 (1980).

[4] K. Hirata, *Nucl. Instrum. Methods Phys. Res. A* **269** (1988) 7. http://dx.doi.org/10.1016/0168-9002(88)90856-X

[5] D. Rice, in *Handbook of Accelerator Physics and Engineering*, Eds. A. Chao and M. Tigner (World Scientific Publishing, Singapore, 1999).

[6] H. Grote, Self-consistent orbits with beam–beam effect in the LHC, CERN-LHC-Project-Report-404 (2000).

[7] E. Keil, Truly self-consistent treatment of the side effects with bunch trains, CERN-SL-95-75-AP (1995).

[8] W. Kozaneki, Impact of beam–beam effects on precision luminosity determination at the LHC, Proc. of the ICFA Mini-workshop on Beam–Beam Effects in Hadron Colliders, Geneva, 2013, Eds. W. Herr and G. Papotti (CERN, Geneva, Switzerland, 2014), p. 227.

[9] M. Schaumann and R. Alemany, in Proc. of the ICFA Mini-Workshop On Beam–Beam Effects in Hadron Colliders, 18–22 March 2013, Geneva, Switzerland, edited by W. Herr and G. Papotti, CERN–2014–004 (CERN, Geneva, 2014), pp. 231–235. http://dx.doi.org/10.5170/CERN-2014-004.231.

[10] W. Herr, Features and implications of different LHC crossing schemes, CERN-LHC-Project-Report-628 (2003).

[11] D. Brandt *et al.*, Is LEP beam–beam limited at its highest energy?, Proc. of the 1999 Particle Accelerator Conference, New York, USA, Vol. 5 (1999), p. 3005.

[12] O. Brüning, in Proc. of the CAS–CERN Accelerator School–Intermediate Accelerator Physics, Zeuthen, Germany, 15–26 September 2003, edited by D. Brandt, CERN–2006–002 (CERN, Geneva, 2006), pp. 129–182, http://dx.doi.org/10.5170/CERN-2006-002.129.

[13] D. Shwartz, in Proc. of the ICFA Mini-Workshop On Beam–Beam Effects in Hadron Colliders, 18–22 March 2013, Geneva, Switzerland, edited by W. Herr and G. Papotti, CERN–2014–004 (CERN, Geneva, 2014), pp. 43–49. http://dx.doi.org/10.5170/CERN-2014-004.43.

[14] M. H. R. Donald and J. M. Paterson, *IEEE Trans. Nucl. Sci.* **26** (1979) 3580. http://dx.doi.org/10.1109/TNS.1979.4330106

[15] J. L. Tennyson, *Flipflop Modes in Symmetric and Asymmetric Colliding Beam Storage Rings*, (Lawrence Berkeley, 1989).

[16] C. Alex, *Coherent Beam–Beam Effects*, SSCL-346 (Superconducting Super Collider Laboratory, Dallas, 1991).

[17] K. Yokoya and H. Koiso, *Part. Accel.* **27** (1990) 181.

[18] Y. Alexahin, *Nucl. Instrum. Methods Phys. Res.* A **480** (2002) 253. http://dx.doi.org/10.1016/S0168-9002(01)01219-0

[19] A. Piwinski, *IEEE Trans. Nucl. Sci.* **26** (1979) 4267. http://dx.doi.org/10.1109/TNS.1979.4330764

[20] H. Koiso *et al.*, *Part. Accel.* **27** (1990) 83.

[21] W. Fischer *et al.*, Observation of strong–strong and other beam–beam effects in rhic, Proc. of the 2003 Particle Accelerator Conference, Portland, USA, Vol. 1, (2003), p.135.

[22] X. Buffat *et al.*, in Proc. of the ICFA Mini-Workshop On Beam–Beam Effects in Hadron Colliders, 18–22 March 2013, Geneva, Switzerland, edited by W. Herr and G. Papotti, CERN–2014–004 (CERN, Geneva, 2014), pp. 227–230. http://dx.doi.org/10.5170/CERN-2014-004.227.

[23] K. Li, Numerical methods, these proceedings.

[24] K. Ohmi *et al.*, *Phys. Rev. Lett.* **92** (2004) 214801.

[25] W. Herr, M. Zorzano and F. Jones, *Phys. Rev. ST Accel. Beams* **4** (2001) 054402.

[26] D. Möhl, in Proc. of the CAS–CERN Accelerator School–Intermediate Accelerator Physics, Zeuthen, Germany, 15–26 September 2003, edited by D. Brandt, CERN–2006–002 (CERN, Geneva, 2006), pp. 245–270, http://dx.doi.org/10.5170/CERN-2006-002.245.

[27] V. A. Lebedev, *AIP Conf. Proc.* **326** (1995) 396. http://dx.doi.org/10.1063/1.47298

[28] V. Kornilov, Passive mitigation, these proceedings.

[29] V. Danilov and E. Perevedentsev, *Nucl. Instrum. Methods Phys. Res.* A **391** (1997) 77. http://dx.doi.org/10.1016/S0168-9002(97)00363-X

[30] E. A. Perevedentsev and A. A. Valishev, *Phys. Rev. ST Accel. Beams* **4** (2001) 024403. http://dx.doi.org/10.1103/PhysRevSTAB.4.024403

[31] S. White *et al. Phys. Rev. ST Accel. Beams* **17** (2014) 041002. http://dx.doi.org/10.1103/PhysRevSTAB.17.041002

[32] X. Buffat, Ph.D. thesis, École Polytechnique Fédérale de Lausanne, 2015.

[33] A. Chao, Beam instabilities in circular machines, in *these proceedings*, 2016.

[34] T. Pieloni, PhD thesis, École Polytechnique Fédérale de Lausanne, 2008.